EMC Modeling of Drives for Aircraft Applications: Modeling Process, EMI Filter Optimization and Technological choice

Baidy-Birame Touré, Jean-Luc Schanen, Laurent Gerbaud, Thierry Meynard, James Roudet, Régis Ruelland

EMC Modeling of Drives for Aircraft Applications: Modeling Process, EMI Filter Optimization and Technological choice

Baïdy Touré[*,***], Jean-Luc Schanen[*], Laurent Gerbaud[*], Thierry Meynard[**], James Roudet[*], Régis Ruelland[***]

* Grenoble Electrical Engineering Lab
UMR 5269 Grenoble-INP – UJF - CNRS, BP 46,
38402 Saint-Martin-d'Hères Cedex, FRANCE

** Laboratoire Plasma et Conversion d'Energie
UMR 5213 INP Toulouse – UPS – CNRS, BP
7122 - 31062 TOULOUSE Cedex FRANCE

*** Liebherr-Aerospace Toulouse SAS, 408,
avenue des Etats-Unis, BP 52010, 31016
TOULOUSE Cedex 2 – France

Paper publication. This paper has been presented at the third IEEE Energy Conversion Congress & Exposition which was held 17-22 September 2011 in Phoenix, Arizona.

Abstract. A new approach for easy and fast modeling of EMI filter in aircraft application is proposed, in order to be used in an optimization process. A modular description in a user friendly environment allows describing the model and taking into account all the technological parameters of the system i.e.: the control strategy, the inverter model (semiconductors, layout, etc.), the filter, the cables and the AC machine. The frequency model is automatically built from this description, as well as its gradients according to its inputs. In a second step, by using this model, an optimization of the filter values can be carried out, using various algorithms, to reach the smallest volume. This early design methodology can also be used to investigate the impact of some technological choices of the electrical drive (control strategy or cable characteristics for instance) on the filter volume.

Keywords. Automatic frequency modelling, EMC, Filter design, Optimization, aircraft application

I. INTRODUCTION

The more electrical revolution in aircraft applications brings a real boost in power electronics research. Indeed, the aeronautic environment requirements are specific, and may necessitate new developments, specific designs, and at least a lot of validations. The More Composite Aircraft is also a new driver for EMC studies. Indeed, this new environment will greatly impact the electromagnetic behavior of the electrical systems, since no "free" shielding will be available on the power harnesses. Thus, there is a strong need in helping the aircraft designers to choose among the various technological possibilities, and to know the impact of these choices on the global weight, cost and volume of the equipment. The EMC filter usually represents roughly 30% of the cost and volume of a power electronics converter, and has consequently to be optimized. Many parameters may impact the sizing of this filter: the converter control law, the choice of semiconductors and/or drivers, the inverter stray elements (inductive and capacitive), the cable selection and placement, the machine characteristics… These impacts should be perfectly known in order to reach a good system design. The paper proposes a pre design methodology, accounting for all technological parameters using simple models. This permits to carry on an optimization process, accounting for all parameters and leading to an estimate of size and weight of the filter. The models are developed in the frequency domain [1-7], including all key sizing parameters. In comparison with previous work, the circuit model is automatically generated, and has not to be specifically developed for a given application.

The approach is very generic: the model of the filter topology, the inverter structure or the cabling configuration can be easily built again and recomputed, thanks to the proposed software architecture. Moreover, the control law is easily taken into account through the source definition used for the static converter. Consequently, the impact of all these elements on the electromagnetic disturbances can be characterized, and the EMI filter optimized. Fig. 1 describes the studied EMI filter between the LISN (Line Stabilization Network) and the SMPS (Switched Mode Power Supply).

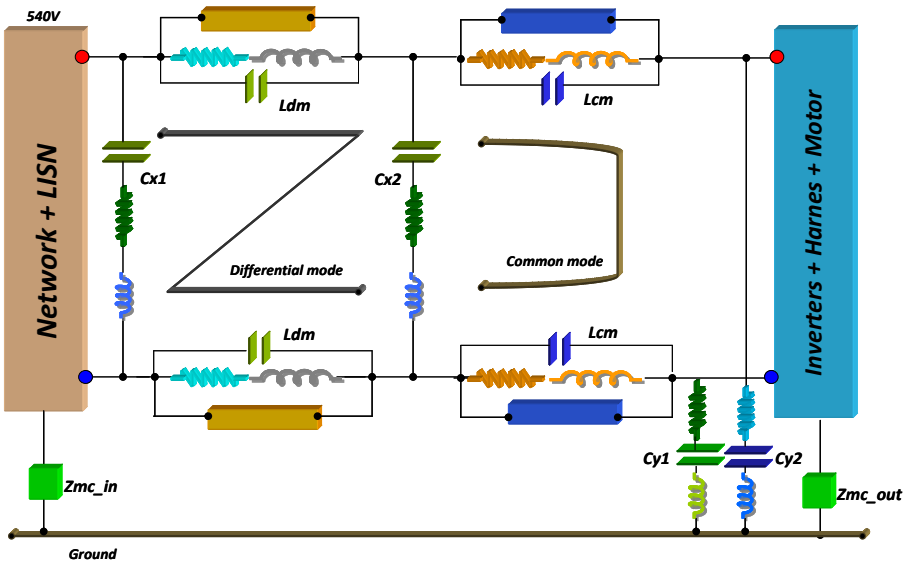

Fig. 1. EMI Filter including stray elements of the components (Differential Mode (right) Common Mode (left))

The paper will first present the model used for the EMC computation, and the tool employed to facilitate its implementation (section II). This model will be validated, in section III, with a simple drive, using experimentally identified parameters. Section IV will detail the other necessary models, used to determine the capacitors and inductors volumes, accounting for magnetic and thermal constraints. The optimization procedure and its implementation in the software environment are provided in section V, as well as the results for one specific case. Section VI contains the conclusion.

This work is supported by

***LIEBHERR-AEROSPACE TOULOUSE SAS 408, avenue des Etats-Unis, BP 52010, 31016 TOULOUSE Cedex 2 – France

II. EMC MODELING

A. *Principle of the Frequency Model*

The EMC equivalent circuit uses high frequency models for each part of the system (electrical components, cables, machine…). The principle of the modeling is to replace the switches by equivalent sources, as presented in several previous works [1-7]. The source characteristics depend on the control law for switching times, and semiconductor technology and drivers for switching wave forms. This circuit is described graphically in a schematic capture. Here, the free version of the PSpice Schematic has been chosen. Then, from the created netlist file, the frequency model is automatically generated as a ICAr software component [8-12].

Fig. 2 shows the example whose will be detailed in this paper. The drive is connected to a Line Impedance Stabilization Network through a DC feeder. The inverter accounts for a DC Link capacitor, a bus bar and the equivalent sources representing the semiconductors. All stray capacitance with the heatsink (connected to the ground) are also taken into account. A Permanent Magnet Synchronous Machine is connected to the inverter through a three-phase harness. It is modeled thanks to an equivalent circuit [1], [4], which values have been obtained by measurements. The identification of the parameters of all models will be provided in section III. The model outputs are the current measured in the DC Feeder, to comply with the Aircraft EMC standards.

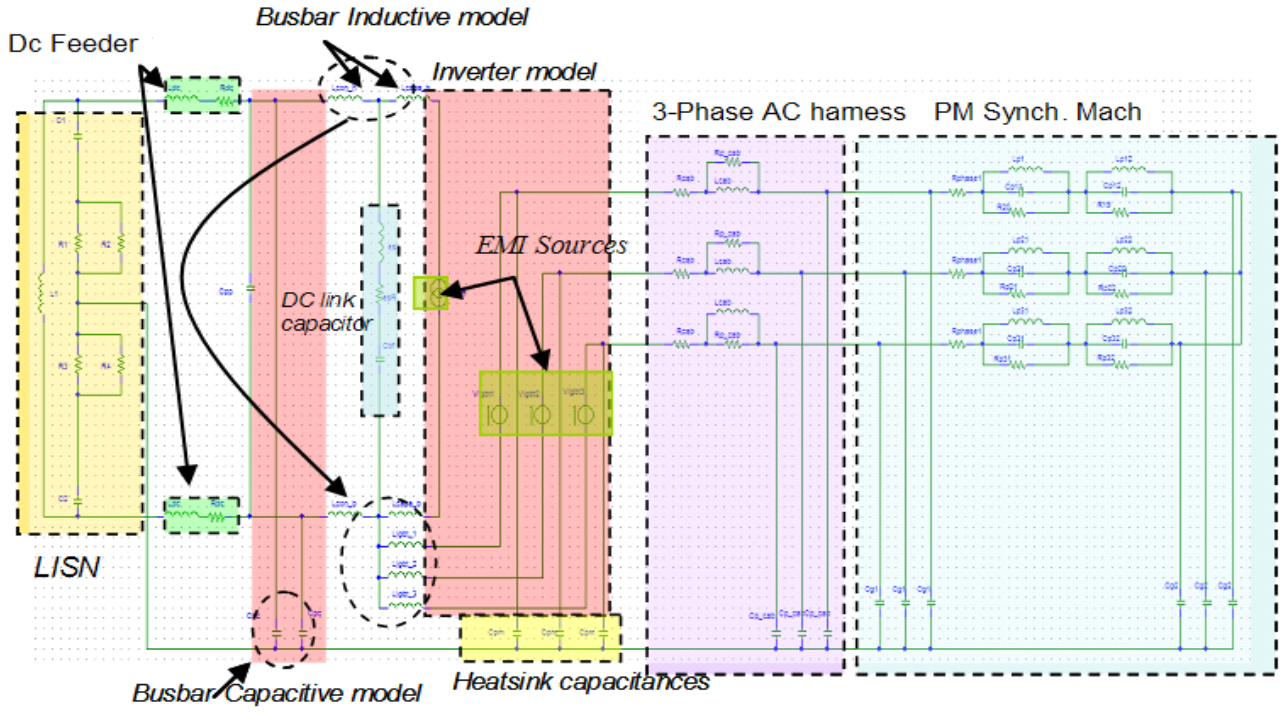

Fig. 2. Illustration of the complete EMC model draw in a simple schematic

B. *Definition of the EMI Sources*

The voltage sources contain both information on control strategy and switching characteristics. They can be obtained from measurements on a prototype, or from accurate time simulations combined with FFT. However, both methods necessitate a careful recording of the signals in the time domain, in order to achieve a correct frequency representation up to several tens of MHz (it is worth noting that both modulus and phase shift are necessary, since several sources are to be combined in the resolution). This does not allow an easy change of the control strategy in the model or optimization. The method presented in the paper disconnects the control strategy from the switching behavior using a reconstitution by convolution of the signals: the switching events are taken from a library (measurements or simulations for given power voltages and currents), and occur at specific times defined by the control law, as illustrated in Fig. 3. This allows an easy change of the control strategy. The graph depicted on Fig.3 shows the comparison of the ideal IGBT voltage (i.e. with ideal switching) and the IGBT voltage after reconstitution (i.e. using the switching events library).

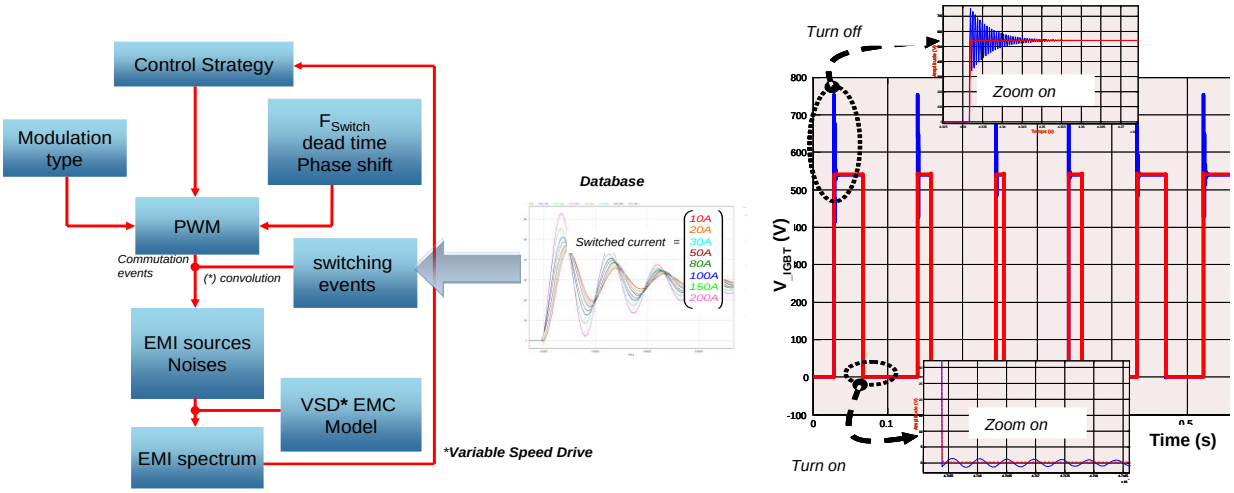

Fig. 3. Elaboration of EMI noise sources. Left: principle – Right: illustration in the time domain (ideal votage -red and Reconstitued voltage -blue).

To validate this approach, Fig.4 provides the two spectra of the reconstructed voltage and the complete common mode waveform obtained using a temporal simulation. They are well superimposed. This is not surprising since the switching database has been based on the temporal simulation. However, this shows that the reconstruction process is well achieved. In comparison with an idealized source using constant rise and fall times (trapeze), the proposed method is more accurate in the high frequency range, since the variation of the switching times is taken into account, as well as voltage overshoots and ringing, or the recovery phenomenon for the current source. The use of an experimental database would be especially interesting since it would correspond to the actual behavior of the semiconductors. Care should be taken in this case to all stray elements and drivers used in the experimental test bench for feeding the database, which would have to be comparable with the one used in the studied drive.

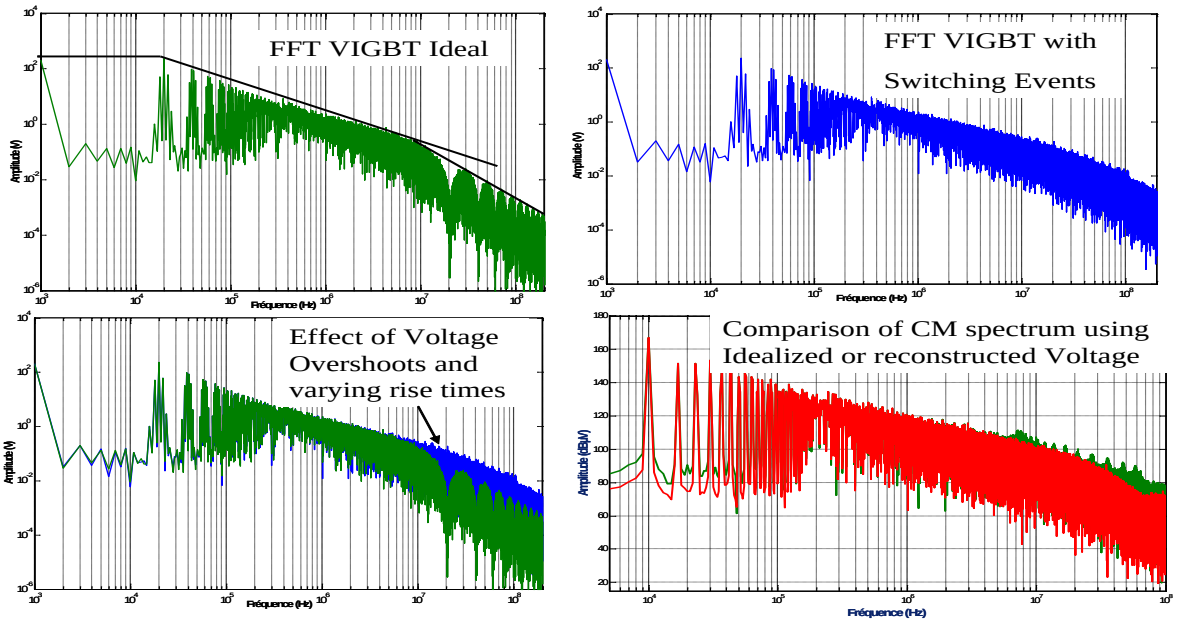

Fig. 4. Comparison of reconstitued (blue) and ideal voltage (green) spectrum and the spectrume of the commun mode voltage.

C. Model generation

The paper proposes to use a new tool [8-12] to create automatically the mathematical model of the system in the frequency domain, using a graphical description of the EMC equivalent circuit drawn by the designer. The gradients of the model outputs

according to the model inputs are also automatically generated. The model is automatically programmed in java language. The definition of outputs variables are simple, as illustrated in Fig. 5.

In addition to the EMC model, the designer adds other equations defining other constraints, e.g.: volume or mass of components, or design constraints in a simple language (only equations, without declarations of the variables). From this complete set of equations, Cades@Generator [8-12] is used to create a software component, supporting the computation of the entire sizing model and its gradients. This ICAr software component is available for calculation and optimization in several computation environments, e.g. Matlab, Cades@Optimizer [8-12], I-Sygth, Excel. For simple calculation or sensitivity analysis, the generated software component can be used in Cades@Calculator [8-12] or Matlab. For optimization, several algorithms can be used, gradient based (SQP-VF13 [13]) or not, in Cades@Optimizer.

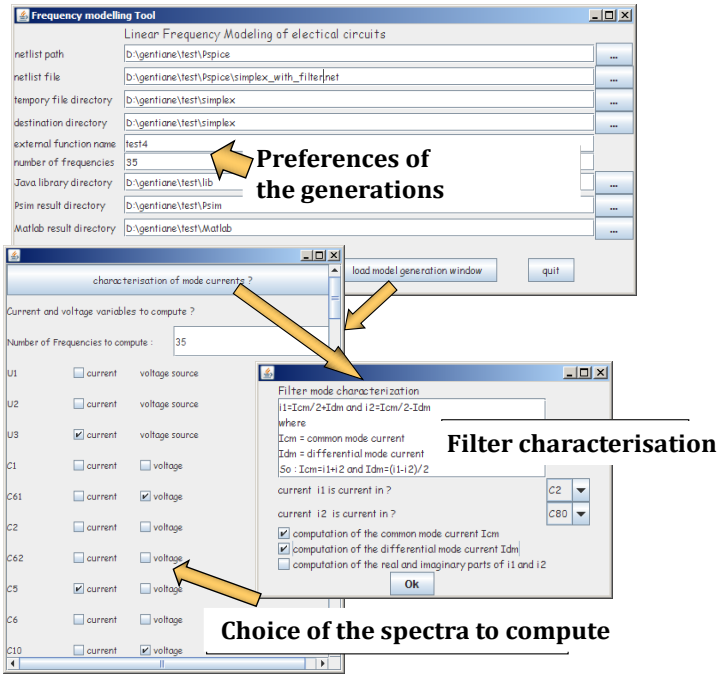

Fig.5. Definition of the frequency model in the frequency model generator

III. MODEL INDENTIFICATION AND VALIDATION

To investigate the accuracy of the generated model using the proposed approach, a comparison has been achieved with measurements on an experimental setup. The model description is modular as illustrated in Fig. 6. Each block brings a contribution to the global EMC model.

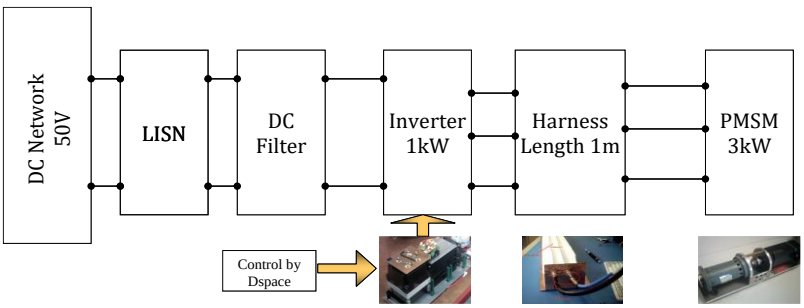

Fig. 6. Modular description of the experimental drive.

The model parameters are extracted from measurements for validation purpose. Fig. 7-Top illustrates the harness identification method. Open and short circuit measurements allow the identification of the per-unit length inductance and capacitance. The main

difficulty is to account for the magnetic coupling between two wires. This one may be especially important when the harness is not shielded. In this case, the magnetic identification uses two measurements: one between one wire and the ground (self inductance) and one paralleling two wires and measuring the equivalent inductance between these cables and the ground. The mutual coefficient between the two wires can thus be extracted, based on Eq.(1) (generic expression valid even for two different wires L_{11} and L_{22}). This procedure can be reproduced several times for multiphase cables if necessary.

$$Lmeas = \frac{L_{11} \cdot L_{22} - M_{12}{}^2}{L_{11} + L_{22} - 2 \cdot M_{12}} \tag{1}$$

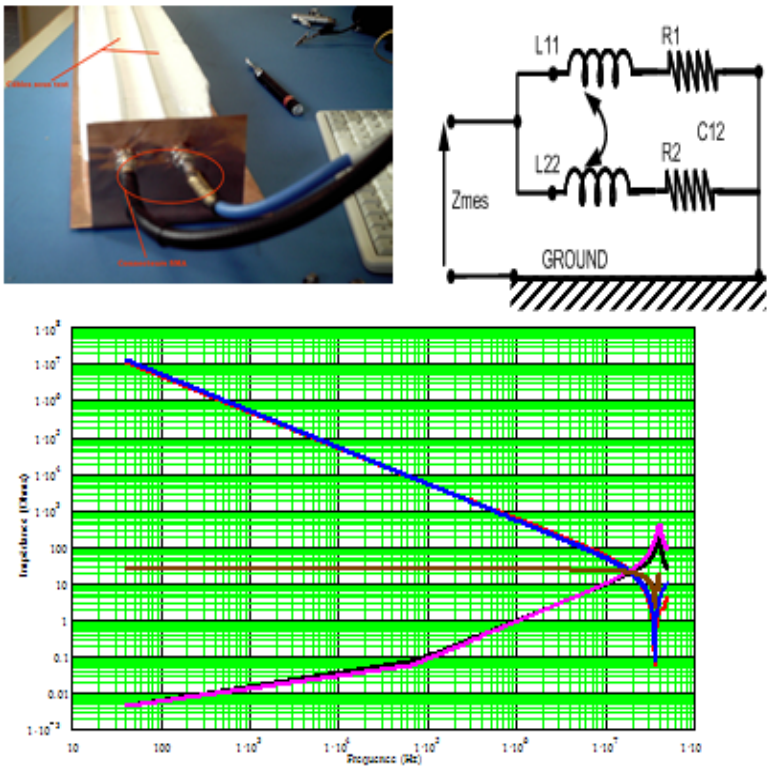

Fig.7. Cable identification procedure

The AC machine has a complex geometry, so a high frequency model is not easy to be obtained from conventional Finite Element Modeling. It has been proposed to obtain the model from measurements, using an impedance measurement bridge and two different configurations: one in common mode (phase to ground) and one in differential mode (phase to phase). The harness can be directly included in the identification, or achieved separately. The complete methodology and justification of the equivalent circuit has been detailed in previous works [1], [4] and will not been included in this paper. It is just illustrated in Fig. 8.

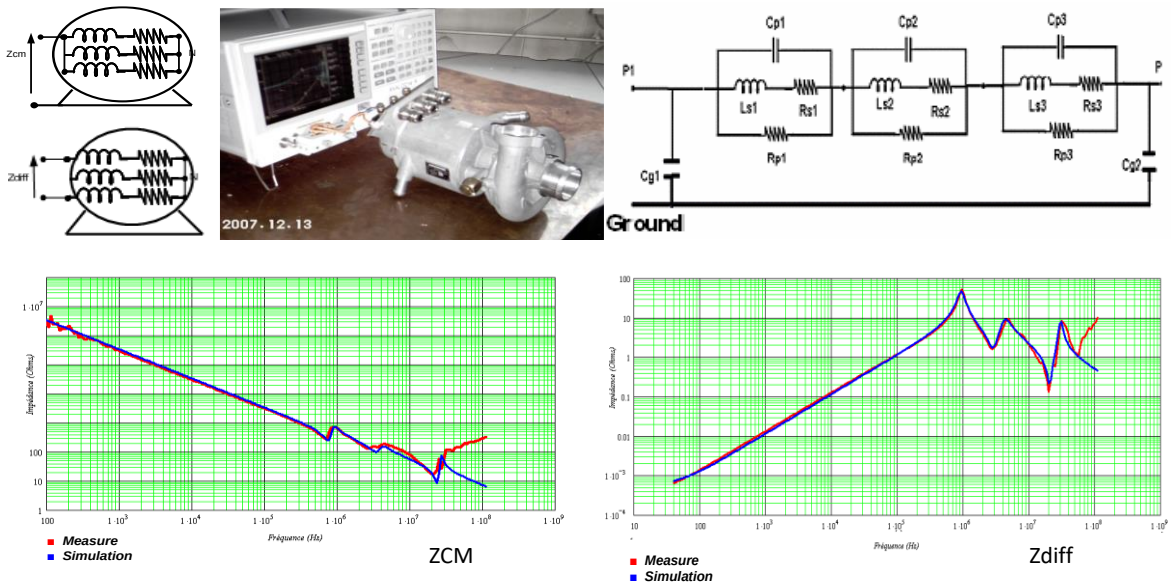

Fig.8. Machine high frequency model and identification procedure.

The identification of the inductive behavior of the interconnects (power package, bus bar model) is achieved with a dedicated PEEC software InCa3D [14] (Fig.9.). The capacitive model is especially important for common mode generation. Stray capacitance matrix can be also extracted from PEEC simulations, as in [15]. In this paper, another method has been proposed, based on an experimental identification. This is especially interesting in many applications where the inverter geometry is not known (in the case it is a provided by a subcontractor and molded in a resin for instance).

The converter exhibits 5 terminals plus the ground which is considered as the reference (2 DC input, 3 AC output and the reference potential –the heatsink-). Thus, its electrostatic behavior can be defined by using 5 independent common mode voltages. In general, for a system with x independent voltages, equation (2) gives the number of required equations in order to estimate all the capacitances and thereby to describe its electrostatic behavior [16].

$$N_{required\_equations} = \frac{x \cdot (x+1)}{2} \tag{2}$$

The full capacitive model should therefore involve 15 capacitors (with 5 independent potentials) according to Eq.(2). However, for simplification purpose, the stray capacitances between conductors have been neglected in comparison with the ground capacitors. Moreover each IGBT is replaced by its output capacitance in the off-state Ci as illustrated in Fig.9. Therefore, the equivalent circuit is composed of 5 common mode capacitances, plus the 6 IGBTs capacitances and the DC link capacitor. The large value of this latter in comparison with the other ones prevents the identification from working properly. Thus, it has been removed. The identification will then result in the differential mode bus bar capacitor, and not the DC bus one. The 6 IGBT capacitors (Ci) have been considered as identical, as well as the AC common mode output ones (Cpm). Therefore, the model presents 5 unknowns: Ci, Cpm, the 2 common mode DC bus capacitors (Cpc1 and Cpc2) and the bus bar differential mode capacitor (Cdc).

Fig.10 illustrates this identification method. 5 measurements have then been used, using some short circuits. These short-circuits allow identifying only paralleled capacitors for every configuration. The aim is to obtain only sums of capacitors so that system to be solved remains linear, leading to a unique solution with only positive values of capacitors.

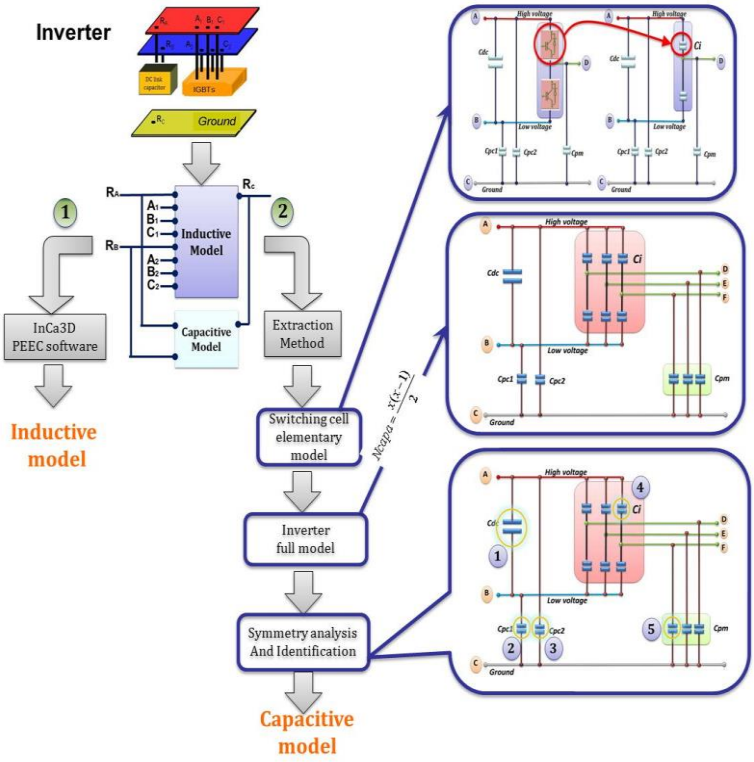

Fig. 9. Synoptic of the identification procedure

The results, provided in Fig.10 have been validated for Ci in comparison with the IGBT datasheet, and for Cdc using a parallel plate formula for the bus bar.

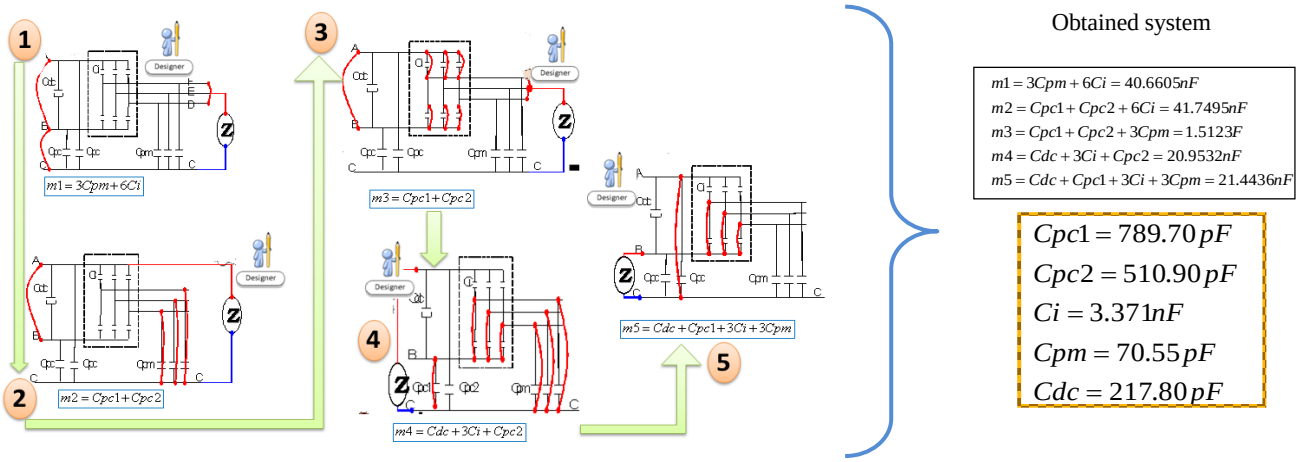

Fig. 10. Inverter capacitive representation (with respect to ground potential) using several impedance measurements for various configurations.

After the identification, the complete EMC model can be validated using the comparison between experimental results (in this case LISN voltage instead of DC feeder currents as proposed by aircraft standards) and simulated one (Fig.11). Obviously, the agreement is good since the model parameters have been identified from the measurements on the experimental setup. However, it proves that the model structure using sources reconstituted by convolution with switching events is valid. This allows using the obtained model in a filter design procedure. The simulation times are dramatically reduced since the computation is simply a linear solving of circuit equations in the frequency domain, and not a step by step solving of differential equations. On a same computer, whereas PSIM time simulation plus FFT needs about 1 hour, the frequency model needs about 10 minutes to compute the whole spectrum from 0.50 to 30MHz.

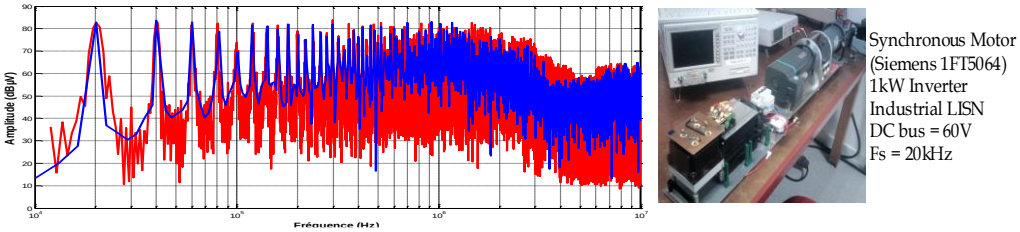

Fig.11. Experimental (red) and simulated EMI spectra (blue) .

IV. MODELS USED FOR FILTER OPTIMIZATION

The last step of the approach is the use of the generated software ICAr component -i.e. the sizing model- in an optimization process. The filter volume has been chosen as the objective function. It is computed taking into account the design of the individual filter components, as detailed hereafter.

A. Capacitors volume expressions

There are two kinds of capacitors mainly used in EMI applications: the MKP-type (polypropylene Cx) for the filtering of the differential mode noise and the MKT-type (polyester Cy) for the common mode noise. The volume of the capacitors can be computed for each type by using a simplified approach, based on parallel plate capacitor formula. In this case, the capacitor volume can be considered as a linear variation according to the capacitance, as shown in Eq. (4). The breakdown voltage U_{xmax} or U_{ymax} impacts the volume in a quadratic way, but it is constant in our application.

$$Volume\_C_{(x,y)} = \frac{C_{(y,x)} * U_{(x,y)\max}^{2}}{\varepsilon_{(x,y)} * E_{(x,y)\max}^{2}} \tag{3}$$

εy, εx are respectively the dielectric permittivities of Cx and Cy. Exmax and Eymax are respectively the maximum dielectric fields in Cx and Cy. Based on this consideration, we decided to suppose a linear variation of the capacitor volume as a function of the capacitance. The linear variation has been fitted to datasheets.

B. Inductors volume expressions and design considerations

The filter inductances are made using toroidal cores. The geometric parameters describing the core (Hcore, Rin, Rout), and the windings (Dc, θ), are described in Fig.12. The magnetic material used will be nanocrystalline soft magnetic materials such as Vitroperm 500F for Common Mode- and KoolMμ for Differential Mode- filter.

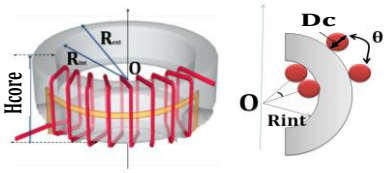

Fig. 12. Filter inductor (toroidal core).

The inductor sizing equations are very similar for Common mode and Differential Mode, and described below.

The inductance value $L_{CM/DM}$ of the CM or DM choke depends on the geometric features of the core (*Ae* the core section, $L_{magnetic}$ the magnetic path length) and the number of turns N per winding.

Additionally, the component has to cope with several constraints, especially avoiding core material saturation and insuring limited losses in the material and in the copper windings. Usually, the sizing of an inductor uses core database. In our case, we considered that all cores are homothetic. We defined two parameters α and β, characterizing the core shape:

$$\alpha = \frac{R_{in}}{R_{out}}; \beta = \frac{H_{core}}{2 \cdot (R_{out} - R_{in})} \tag{4}$$

Therefore, all homothetic cores can be deduced from an initial one by varying one geometric parameter only, H_{core}, keeping α and β constant ($\alpha = 0.62$, $\beta = 1.47$). D_{in} and D_{out} and Ae can be deduced from H_{core}, α and β, as shown hereafter.

$$Ae = \frac{H_{core}{}^2}{2 \cdot \beta} \tag{5}$$

$$L_{magnetic} = \frac{\pi \cdot H_{core}}{2 \cdot \beta} \cdot \frac{1+\alpha}{1-\alpha} \tag{6}$$

Obviously, this may generate a non existing core, but this will not be far from an actual one, and this allows converging easier, close to an available solution in the optimization process. So, using this representation, the time of the optimization loop is greatly reduced.

The analytical equation linking the geometric parameter H_{core} and the turn number N per winding to the inductance value (L_{CM} or L_{DM}) is as follows:

$$L_{CM/DM} = N^2 \cdot \mu_0 \cdot \mu_r \frac{Ae}{L_{magnetic}} \Rightarrow L_{CM/DM} = \frac{N^2 \cdot \mu_0 \cdot \mu_r}{\pi} \cdot \frac{1-\alpha}{1+\alpha} \cdot H_{Core} \tag{7}$$

Besides, the leakage inductance of the inductor, which for EMC filter is composed of two wirings, is another critical parameter of the inductor design and can be directly expressed by Eq. (8) [17-18]. In this relation, $\sigma_{winding}$ is the angle that a winding subtends on the core in degrees. $\sigma_{winding} = 170°$ for CM, and 150° for DM. These values have been considered as conventional for EMC components.

$$L_{leakage} = \frac{\mu_0 \cdot \mu_R \cdot N^2 \cdot Ae}{L_{magnetic} \cdot \sqrt{\frac{\sigma_{winding}}{360} + \frac{\sin\left[\frac{\sigma_{winding}}{2}\right]}{\pi}}} \tag{8}$$

For simplification, the inductor size will be considered as the core size only (even if the model may be improved by adding the wiring volume).

$$Vol_L = H_{core}{}^3 \cdot \frac{\pi}{4 \cdot \beta^2 \cdot (1-\alpha)^2} \tag{9}$$

One of the limiting factors in inductor design is to avoid saturation. Therefore, the maximum induction has to be monitored. It depends on the peak current in the inductor $\hat{I}$, using Eq. (10). It is worth noting that this constraint does not use the same equation for DM and CM inductor. With nanocrystalline, the B_{max} peak induction has been taken at 1.2T. With KoolMµ, it has been chosen at 0.7T.

$$B_{max} = \frac{L_{CM} \cdot \hat{I}}{2 \cdot N \cdot Ae} \tag{10}$$

For differential mode inductance, the peak current $\hat{I}$ can be considered as the DC current plus the ringing current. This one depends on the filter value. For the moment, an analytical model to obtain this value is still under development. Therefore, this ringing current has been kept constant during optimization. Its value is the one obtained for a simulation with a filter respecting the EMC standard (50 mA).

For common mode inductor, Eq. (10) may not be sufficient, since the leakage flux may avoid the compensation between the two windings. Knowing that the Common Mode Inductor is a coupled inductor L_{CM}, with primary current equal to $I_{DM}+I_{CM}/2$, and a secondary current equal to $-I_{DM}+I_{CM}/2$, since the turn number are equal, leads to the following representation (Fig.13). The expression of the magnetic flux per winding, based on this representation, is defined by Eq. (11):

$$\phi_1 = L_1 \cdot \left(I_{DM} + \frac{I_{CM}}{2}\right) + M_{21} \cdot \left(-I_{DM} + \frac{I_{CM}}{2}\right) \Rightarrow \phi_1 = (L_1 - M_{21}) \cdot I_{DM} + (L_1 + M_{21}) \cdot I_{CM}/2 \text{ and } \phi_2 = (-L_2 + M_{12}) \cdot I_{DM} + (L_2 + M_{12}) \cdot I_{CM}/2 \tag{11}$$

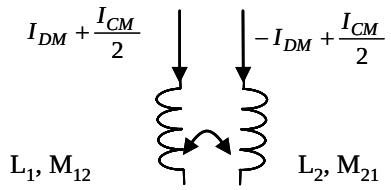

Fig.13. Electrical representation of a CM inductor.

The total flux in the core is thus:

$$\phi_{tot}=\phi_1+\phi_2=I_{DM}\cdot(L_1-L_2)+\frac{I_{CM}}{2}\cdot(L_1+L_2+M_{12}+M_{21}) \tag{12}$$

The first term of (12) corresponds to the difference of DM flux, in other words to the leakage flux. Since this one can be expressed using the leakage inductance [19-20], evaluated with (8), Eq. (12) can also be expressed as follows using $M = M_{12} = M_{21}$:

$$\phi_{tot}=I_{DM}\cdot L_{leakage}+\frac{I_{CM}}{2}\cdot(L_1+L_2+2\cdot M) \tag{13}$$

Therefore, considering $L_1 \approx L_2$, the total flux in the CM choke is $(L_1+M).I_{CM}$, plus a corrective term $L_{leakage}.I_{DM}$, accounting for leakage flux. Note that $L_{CM} = L_1+M$ is the equivalent common mode. The peak induction Bmax in the magnetic material can thus be monitored and is a constraint during the optimization process. As for DM inductor, the CM peak current is fixed at a constant value (150 mA). As for DM current ripple, this value comes from a simulation with a well designed CM filter.

The inter-winding capacitance of inductor induces mainly resonances in high frequency range and reduces the effectiveness of the EMI filter. It is essential to estimate its value. The latter is computed by using Eq. (14) [21].

$$Epc=1.366\cdot\varepsilon_0\pi\cdot L_{turn}\left[\frac{\varepsilon_R\theta}{\ln\left[\frac{D_{ext}}{D_{int}}\right]}+\cot\left[\frac{\theta}{2}\right]-\cot\left[\frac{\pi}{12}\right]\right] \text{ where } \theta=a\cos\left[1-\frac{\log\left[\frac{Dext}{D\,\mathrm{int}}\right]}{\varepsilon_R}\right] \tag{14}$$

where Dext is the diameter of a wire turn with insulator and Dint without insulator, Lturn is the length of a turn.

The wire diameter is chosen according to the maximum allowed current density, Jc, which is one degree of freedom in the inductor design.

The last constraint is now related to the losses in the inductor. The copper losses are estimated using the serial resistance Rs of the inductor given by Eq. (15) from Levasseur formula in the case of circular conductors. Rdc is the resistance at low frequencies. Dc is the conductor diameter, ρ is the resistivity of the conductor, Ac is the copper section and δ is skin depth. The copper losses can thus be expressed using Eq. (16).

$$Rs=Rdc\left[1+0.25+\sqrt[6]{0.18+\left[\frac{Ac}{\pi\cdot D_c\cdot\delta}\right]^6}\right] \text{ where } Rdc=\frac{4\rho NL_{turn}}{\pi D_c} \tag{15}$$

$$P_{Copper}=Rs\cdot I_{rms}^2 \tag{16}$$

The core losses are valued using the IGSE (Improved Generalized Steinmetz Method) [22], Eq. (17). k, αs βs are the material parameters from manufacturers.

$$\left\langle P_{Core}(t)\right\rangle=\frac{1}{T}\int_0^T k_1\cdot\left|\frac{dB_{Total}}{dt}\right|^{\alpha s}\cdot\Delta B^{\beta s-\alpha s}\cdot dt \tag{17}$$

$$k_1=\frac{k}{(2\pi)^{\alpha s-1}\int\left|\cos\theta\right|^{\alpha s}\cdot 2^{\beta s-\alpha s}\cdot d\theta}$$

The total inductor losses (P_{Copper} + P_{Core}) can be limited during the optimization process, either at a maximum value, or through a maximum temperature, using a thermal model. This one is presented in the following section.

C. *Temperature rise estimation*

The thermal model is the last step of the inductor design. It supposes that heat is transferred from the surface of the inductor to ambient by natural convection and radiation. The Newton law gives the following relation:

$$\Phi_{Conv} = H \cdot S(T_r - T_{amb}) \tag{18}$$

where H is the convection coefficient, S the heat exchange surface and T_r-T_{amb} the temperature rise.

Considering a toroidal core, there are four surfaces for heat transfer, namely S_{ext}, S_{int}, S_{top}, S_{bottom}.

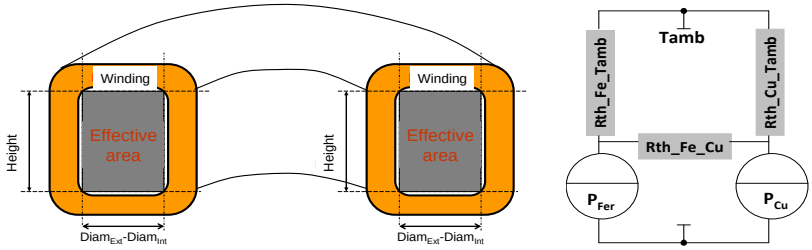

Fig. 13. Geometric model and the height eB of the winding for toroidal shaped core and thermal model

$$\begin{aligned}
S_{ext} &= \pi \cdot (D_{ext} + 2 \cdot eB) \cdot (H_{haut} + 2 \cdot eB) \\
S_{int} &= \pi \cdot (D_{in} - 2 \cdot eB) \cdot (H_{haut} + 2 \cdot eB) \\
S_{sup} &= \frac{\pi}{4} \cdot \left[(D_{ext} + 2 \cdot eB)^2 - (D_{int} - 2 \cdot eB)^2 \right] = S_{inf} \\
eB &= \frac{1}{2} \cdot \left[D_{int} - \sqrt{D_{int}^{\ 2} - \frac{N \cdot D_{spire}^2}{kbob}} \right]
\end{aligned} \tag{19}$$

In the same way, the convection heat transfer coefficient is made with H_{ext}, H_{int}, H_{top}, and H_{bottom} where

$$\begin{aligned}
H_{int} &= 1.42 \cdot \left[\frac{T_r - T_{amb}}{H_{height} + 2eB} \right]^{0.25} = H_{ext} \\
H_{inf} &= 0.66 \cdot \left[\frac{T_r - T_{amb}}{D_{ext} - D_{int} + 2eB} \right]^{0.25} \\
H_{sup} &= 1.32 \cdot \left[\frac{T_r - T_{amb}}{D_{ext} - D_{int} + 2eB} \right]^{0.25}
\end{aligned} \tag{20}$$

These parameters are computed with respected to the thermo-physical properties of the air film at 300°K [23]. The convection heat transfer coefficient is given by

$$H = \frac{N_u}{L_c} \lambda \tag{21}$$

where Nu is the Nusselt number, Lc the characteristic length of the heat transfer surface and λ the thermal conductivity.

Eq. (21) is carried out thanks to some mathematical considerations and simplification. For the radiated flux, the Stefan law gives:

$$\Phi_{Rad} = \sigma \cdot \varepsilon \cdot S(T_r^4 - T_{amb}^4) \tag{22}$$

Finally the power dissipated is equal to the heat transfer as given below:

$$\Phi_{Conv} + \Phi_{Rad} = P_{Copper} + P_{Core} \tag{23}$$

So, the solving of this four-order polynomial equation for Tr gives an estimation of the actual surface temperature of the inductors.

Now the optimization problem can be entirely described in the software environment.

V. FILTER OPTIMIZATION

A. *Optimization problem definition*

The filter has to be designed to meet the aeronautical standard DO-160E [24], which is required in our aircraft application. The filter components have to fulfill the design constraints (Peak Induction, max losses or temperature increase, …). The objective function is the filter volume. To check the EMC constraints, a vector of fifty frequencies has been monitored, in the range [150 kHz - 30MHz].

This is illustrated by Eq.(24)

$$
\begin{aligned}
&if\ \left|Spectrum(Freq,X)\right| > DO160E(Freq)\ then\\
&\quad \sigma(Freq,X) = \left|Spectrum(Freq,X)\right| - DO160E(Freq)\\
&else\\
&\quad \sigma(Freq,X) = 0\\
&endif\\
&Fobj = \min(Volume(L,C) + \sigma(Freq,X))
\end{aligned}
\tag{24}
$$

The optimization variables will be described by a vector of 6 parameters: two capacitors Cx, Cy and two inductors defined each one by a geometrical parameter (Hcm and Hdm), a winding turn number (Ncm and Ndm) and the maximum allowed current density in the inductors (J_c). $X = [Hcm, Ncm, Hdm, Ndm, Cx, Cy, J_c]$

The complete chart for the EMI filter optimization procedure implemented in CADES is illustrated in Fig.14. Various optimization algorithms can be used and compared. For simple calculation, the ICAr component can be used in Cades@Calculator or Matlab. For optimization, this components has been generated with the associated gradients, therefore, it can be used with many algorithms (SQP-VF13, Discrete Optimizer (DO), and Evolution Strategy (ES)). In this paper, the discrete optimizer (DO) is mixed with Evolution Strategy algorithm (ES) [25] to take into account the discrete parameters.

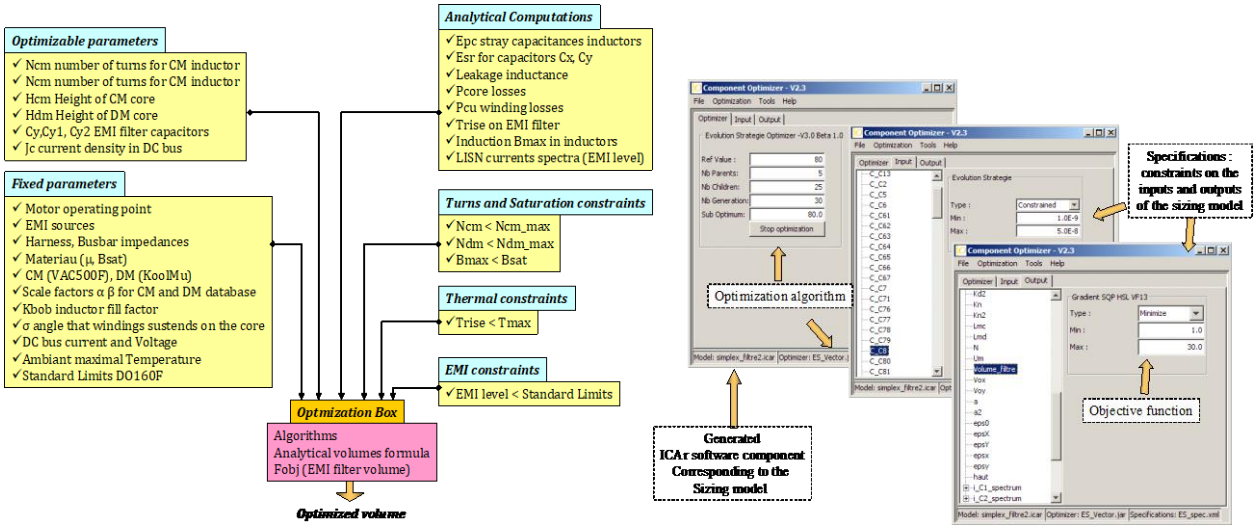

Fig.14. Cades@Optimizer: Optimization Process.

B. Optimization results

Some results are given in Fig. 15 and Tables I and II, in the case of a simple 1 kW a drive. In comparison with the initial filter, designed with usual methods, the volume reduction is obvious (33%). It is clear that the low frequency spectrum is the closest to the standard. This is normal since the low frequency attenuation necessitates a high inductor value. Therefore; the smallest margin has to be considered to optimize the filter volume. As soon as the standard is no more limited (below 150 kHz), the spectrum is allowed to increase. Indeed, the optimized filter presents significantly larger low-frequency content compared to the baseline filter. As mentioned before, this is due to the low impedance of the optimized filter which has a high cutoff frequency. In this study, we did not account for lower frequencies standards, which may also be taken into account. For instance, we may add an additional constraint to avoid the instability of the DC network, what is also linked to the filter input impedance. Should this additional constraint be added, this may result in another optimization result. Another solution may be to add a damping circuit to the EMI filter [26], in order to reach higher attenuations in the low frequency range (below 150 kHz). However, this is outside of the scope of this paper.

Beside, this developed optimization tool allows a very easy change in the circuit topology, since the model description starts from a graphical description, and the model generation is automatic and fast. This allows for instance a convenient change of the filter

topology if desired, in particular to take into account a damping circuit if needed. This one could be automatically optimized in the process.

The analysis of the optimization results also shows that the DM filter represents almost 42% of the EMI filter total volume in the obtained solution. The computed gradients can also provide important information about the sensitivity study. For instance, in Fig. 16 the gradient model corroborates that the importance of Hdm parameter is about 12.7% for the total volume of the filter, in comparison with the other parameters of the model. So, it would be interesting to guide the optimization on the differential mode filter parameters to minimize it. In particular, another control law should be able to reduce its size.

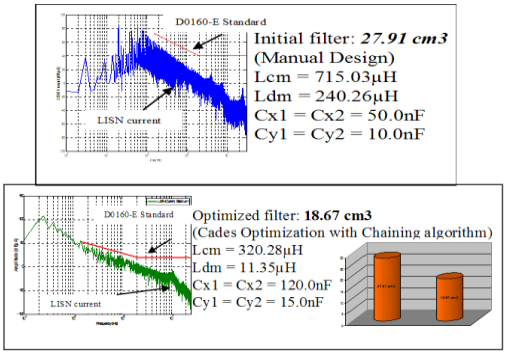

Table I: Common Mode Filter Lmc = 320µH *(Optimized Choke Volume 5.27cm³)*

$L_{leakage}$ (µH)	Bcore (T)	2*N (turns)	Losses (mW)	Ae (mm²)	Le (mm)	Di (mm)	Do (mm)	T (°C)	Epc (pF)
7.98	0.73	16	620	14.2	37.63	9.42	14.5	71	3.40

Table II: Differential Mode Filter Lmd = 11.35µH *(Optimized Volume 7.85cm³)*

$L_{leakage}$ (nH)	Bcore (T)	2*N (turns)	Losses (mW)	Ae (mm²)	Le (mm)	Di (mm)	Do (mm)	T (°C)	Epc (pF)
45.69	0.56	12	467	24.9	38.42	8.1	16.30	64	5.26

Fig. 15. LISN current spectrum using manual design (blue) and developed optimization tool (green).

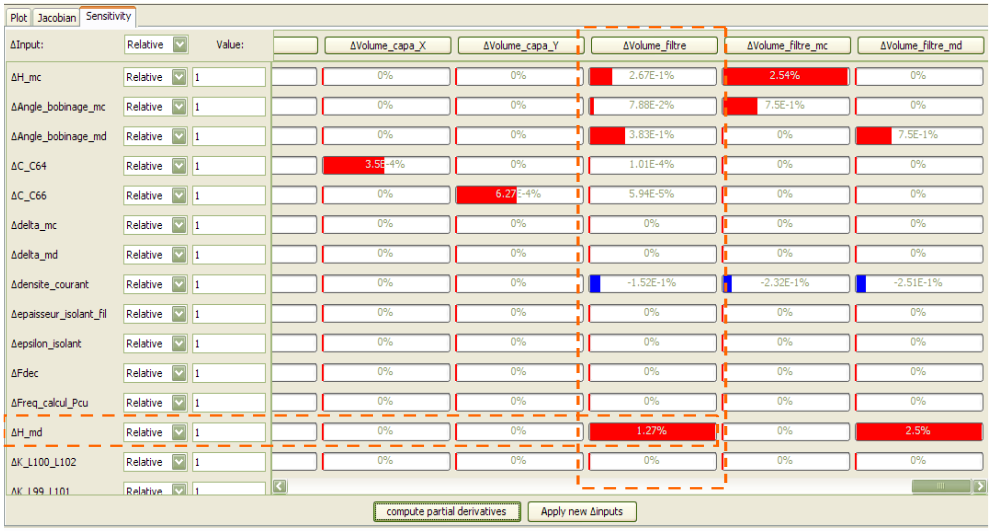

Fig. 16. Gradient model computed.

VI. Conclusion

This paper has shown a complete implementation of an EMC model in the frequency domain of any kind of drive. A modular description and a complete automatic model generation facilitate the use by the designer. The source description accounts separately for the control law and the switching characteristics thanks to a switching library and a waveform reconstitution. Model identification can be based on simulation or measurements.

A measurement method for inverter stray capacitances extraction has been presented, as well as for the other components. An EMC filter volume optimization can then be performed easily. Even if the proposed models for inductor design are not the most accurate, and can still be improved, the optimization method has been proven. The modular description and the convenient way to describe sizing equations allow very easy improvement.

Acronyms

EMI	ElectroMagnetic Interferences	*SQP*	Sequential Quadratic Programming
EMC	ElectroMagnetic Compatibility	ES	Evolutionary Strategy
DM	Differential mode	*CADES*	Component Architecture for the Design of Engineering System
CM	Common mode		
LISN	Line Impedances Stabilization Network	*Icar*	Interface Component Architecture
DO-160E	Aeronautic Standard	*PEEC*	Partial Equivalent Element Circuit
PMSM	Permanent Magnet Synchronous Motor	*InCa3D*	Inductance Calculation 3D software
IGBT	Insulated Gate Bipolar Transistor	*PSIM*	Power Simulation software

Index of symbols

Emax	Dielectric strength	*Sext, Sint, Sout, Sint*	Heat transfer surfaces
Umax	Breakdown voltage EMI filter capacitor	*Volume_C*	Capacitors volume
Cx_1, Cx_2	Capacitors for differential mode filter	*Volume_L*	Inductors Volume
Cy	Capacitors for common mode filter	*Ci*	IGBT capacitance in state-off
ε_R	Permittivity of the dielectric	*Cpm*	Capacitance between the middle point of switching cell and the heatsink
ε_0	vacuum permittivity		
Lcm	Common mode inductance	*Cdc*	Differential capacitance between high voltage and low voltage phase
Ldm	Differential mode inductance		
Icm	Common mode current	*Cp1, Cp2*	Capacitance between the high voltage phase, low voltage phase and the ground
Idm	Differential mode current		
Hcore	Height of a magnetice core	μ_R	Relative magnetic permeability
Din	inner diameter of a magnetice core	μ_0	Magnetic permeability of free space
Dout	outer diameter of a magnetice core	*Nu*	Nusselt number
Ae	Core effective area	*Lc*	Characteristic length of the heat transfer surface
$L_{magnetic}$	Average mean path length	λ	Thermal conductivity
Lleakage	Leakage inductance of a winding	*kcm*	Magnetic coupling coefficient
M	Mutual inductance of windings	*Ï*	Peak current
Rdc	Winding DC resistance	δ	skin depth
Rac	Winding AC resistance	*Irms*	RMS current in the winding
Rs	Serial resistance of a winding	*K, αs, βs*	Steinmetz loss coefficients
Ac	Wire section	*eB*	height of the winding for toroidal
Dc	Wire diameter	σ	Winding angle
N	Number of turns per winding	ρ	resistivity of copper
Bmax	Saturation flux density	α, β	scale factor of the magnetic material
Bcm	Common mode current generated flux density	*Pvol*	Core losses per volume
S	Heat exchange surface	*Pcopper*	Winding losses
T_r	Temperature rise	*Rth*	Thermal resistance
Tamb	Ambiant temperature	*H*	Convection coefficient

VII. REFERENCE

[1] Revol B., Roudet J., Schanen J.L., Loizelet P. "EMI study of a three phase inverter-Fed Motor Drives, IEEE trans on IAS, Jan/Feb 2011.

[2] Hartmann, M.; Ertl, H.; Kolar, J. W.; , "EMI Filter Design for a 1 MHz, 10 kW Three-Phase/Level PWM Rectifier," Power Electronics, IEEE Transactions on , vol.26, no.4, pp.1192-1204, April 2011

[3] F. Wang, W. Shen, D. Boroyevich, S. Ragon, V. Stefanovic, M. Arpillere “Design Optmizatio of industrial Motor Drive Power stage using genetic algorithms”, 41st IAS annual meeting, vol 5, October 2006, pp 2581-2586.

[4] Revol B., Roudet J., Schanen J.L. Loizelet P. "Fast EMI prediction method for three-phase inverter based on Laplace Transforms", Conference record of the 2003 IEEE, PESC 2003, Acapulco, Mexico.

[5] F. Costa, C. Vollaire, R. Meuret, “Measurements and Simulation of Common Mode Conducted Noise Emissions in Adjustable-Speed AC” Proceedings, 20th Int. Zurich Symposium on EMC 2009.

[6] Ran & al., "Conducted Electromagnetic Emissions in Induction Motor Drive Systems Part II: Frequency Domain Models", IEEE trans on power electronics, Vol 13 n°4, 1998

[7] Chen & Al. "Towards EMI Prediction of a PM Motor Drive for Automotive Applications", APEC 2003

[8] L.Gerbaud, B.Touré, JL.Schanen, "Modelling Process and Optimisation of EMC Filters for Power electronics Applications", OIPE 2010, 14-18 septembre 2010, Sofia, Bulgarie

[9] B. Touré, JL. Schanen, L. Gerbaud, T. Meynard, JP. Carayon, “EMC Modeling of Drives for Aircraft Applications: Modeling Process and Optmization of EMI Filters” EPE 2011, 29 Août-1 September, Birmingham.

[10] P. Enciu, F. Wurtz, L. Gerbaud, B. Delinchant, “AD for Optimization in Electromagnetism Applied to Semi-Analytical Models Combining Composed Functions”, COMPEL : The International Journal for Computation and Mathematics in Electrical and Electronic Engineering, special issue on selected paper from OIPE’2008, 2009, Volume 28 Issue 5

[11] P. Enciu, L. Gerbaud, F. Wurtz, " Automatic Differentiation Applied for Optimization of Dynamical Systems", IEEE Transactions on Magnetics, ISSN: 0018-9464, Vol. 46, Issue 8, August 2010, pp. 2943-2946

[12] B. Delinchant, D. Duret, L Estrabaut, L. Gerbaud, H. Nguyen Huu, B. du Peloux, H.L. Rakotoarison, F. Verdiere, F. Wurtz, "An Optimizer using the Software Component Paradigm for the Optimization of Engineering Systems", COMPEL, the international journal for computation and mathematics in electrical and electronic engineering, special issue : selected paper from the 9th workshop on optimisation and inverse problems in electromagnetics, Sorrento, 2006, Volume 26, Number 2, 2007, pp 368-379

[13] VF13. Available on http://www.hsl.rl.ac.uk/index.html

[14] http://www.cedrat.com/en/software-solutions/inca3d.html

[15] Ardon, V.; Aime, J.; Chadebec, O.; Clavel, E.; Vialardi, E. "MoM and PEEC Method to Reach a Complete Equivalent Circuit of a Static Converter", Electromagnetic Compatibility, 2009 20th International Zurich Symposium on, 2009

[16] JL Kotny, X. Margueron, N. Idir, High Frequency Modeling Method of EMI filters, IEEE ECCE 2009.

[17] Mark J Nave “On the modelling Common Mode Inductor” Electromagnetic Compability Symposium 1991 Aug 1991

[18] M. Heldein, L. Dalessandro, W. Kolar ‘The three phase common mode inductor: Modeling and Design issues”, IEEE Tansactions on Power Electronics, vol 58, n°8, Aug 2011, pp 3264-3274.

[19] Zhu, G.; McDonald, B. A.; Wang, K.; , "Modeling and Analysis of Coupled Inductors in Power Converters," Power Electronics, IEEE Transactions on , vol.26, no.5, pp.1355-1363, May 2011

[20] A. Roc’h, H. Bergsma, D. Zhao, B Ferreira, F. Leferink ”Performance Optimization aspects of common mode chokes”, 19th international Zûrich Symposium on Electromagnetic Compatibility, 19-22 May 2008, Singapore

[21] Massarini, A. Kazimierczuck, M.K “Self capacitance of inductors”, Power Electronics, IEEE Trans. on, 1997

[22] Sullivan, Harris, Herbert "Core loss predictions for general PWM waveforms from a simplified set of measured data" in Proc. of Applied Power Electronics Conference and Exposition (APEC)

[23] M. Sippola, E. Sepponen “Accurate Prediction of High Frequency Power-Transformer Losses and Temperature Rise”, IEEE trans on IAS, vol. 17, 5 September 2002

[24] “Environmental Conditions and Test Procedures for Airborne Equipment”, RTCA/DO160E, RTCA Inc. 2004.

[25] Available at ftp://math.nist.gov/pub/Jampack/Jampack/.

[26] Xing, L.; Sun, J.; , "Optimal Damping of Multistage EMI Filters," Power Electronics, IEEE Transactions on , vol.27, no.3, pp.1220-1227, March 2012